COMPUTATIONAL OPTIMIZATIONS TOWARDS AN ACCURATE AND RAPID ELECTROMAGNETIC EMISSION MODELING

A. Ramanujan, Z. Riah, A. Louis, and B. Mazari

Research Institute in Embedded Systems (IRSEEM)
Technopôle du Madrillet, Avenue Galilée, BP 10024
Saint Etienne du Rouvray 76801, France

Abstract—In this paper, a parametric electromagnetic radiated emission model has been explored. Several mathematical improvements with respect to its extraction and computational performance have been deployed. The model, represented with an array of radiating electric dipoles, predicts the electromagnetic emission of components and systems. Core-level changes have been made in order to extract the model parameters: the dipole positions, their orientations and currents, and the effective relative permittivity from near-field measurements. Thresholding and windowing techniques are used to detect and optimize dipole positions, directly from the field data. A fast and memory efficient two-level optimization algorithm based on the Levenberg-Marquardt non-linear least squares technique is implemented for parametric extraction. All the constraints of the previous model have been overcome and the system is validated for mono-substrate and multi-substrate devices from measurements and/or simulations, with promising results. A tremendous improvement in modeling capability and performance has been obtained when compared with that of its erstwhile counterpart.

1. INTRODUCTION

Electromagnetic compatibility (EMC) modeling has been a hot topic for a while now in various departments of electrical and electronics engineering. Numerical modeling techniques to tackle a wide range of practical problems have been of utmost interest to researchers and industries. The current trend is to target EMC at component level and

thus predict the device's electromagnetic behavior during the design stage itself. Radiated emission from a system is an important EMC phenomenon that not only affects the system's performance, but also that of neighboring devices.

Considering the densely integrated electronic systems used today, it is necessary to build simple models representing the radiation behavior of components and systems. The models developed in [1–7] show comprehensive details on the recent advances in "device-level" EMC radiated emission modeling. In particular, the models in [3–7] represent the electronic component under test with a set of electric and/or magnetic dipoles and are capable of predicting the radiated electromagnetic emissions of the device. The model parameters are either extracted from near-magnetic field measurements and/or near-electric field measurement. The recently developed model [4] which was inspired from a previous model [3], implements an iterative extraction procedure for determining its parameters.

In contrast to the models developed in [6, 7], this model is built using a set of electric dipoles and is extracted from near-magnetic field measurements. It also incorporates the role played by the effective relative permittivity (ϵ_{reff}) on the radiated electromagnetic fields in its modeling procedure. The model requires that the value of ϵ_{reff} has to be provided prior to extraction. Additionally, due to the presence of a single dipole type, it is easily integrable into commercial 3D simulation tools as reported in [8, 9]. The model has been validated on several microwave devices [4] and "on-chip" devices [5] of very small dimensions (area $\approx 10 \, \text{mm}^2$) used very commonly in RF systems-in-package and system-on-chip devices.

The model is robust and versatile than its earlier counterparts, but has a few constraints: the iterative extraction procedure is computationally intensive, the knowledge of the substrate present in the device under test is needed beforehand and the dipole positions are not optimized since they are pre-fixed. To overcome these inconveniences, several mathematical improvements have been implemented to upgrade the modeling procedure towards a fast and a memory efficient one. The Jacobian of the system representing the model is predetermined and in-built within the extraction method. The dipole positions are extracted and optimized using the intensity thresholding technique, combined with an optional windowing technique. The model parameters are determined in a two-step optimization procedure: the first-level optimization extracts the dipole parameters and the second-level extracts the ϵ_{reff} at all points in space. The tangential near-magnetic field and the near-normal electric field measurements are used for parameter extraction. The non-

linear system is split into real and imaginary parts and optimized simultaneously.

The model and the newly improved parametric extraction procedure are explained in detail in this paper. The model is validated on a couple of simple devices, built on a single substrate and complex devices possessing multiple substrates, operating in microwave frequency ranges. The optimized number of dipoles and the computational advantages of the model are also discussed in detail.

2. ELECTROMAGNETIC EMISSION MODEL

2.1. Presentation of the Existing Model

The model is represented with a set of elementary electric dipoles placed on the x-y plane as shown in Figure 1 [4]. Each dipole in the network is represented by its position, its orientation with respect to the x-axis ($\theta \in \mathbb{R}$), its length ($d\ell \in \mathbb{R}$) and the current flowing through it ($I \in \mathbb{C}$). This model, in itself, is an improved and optimized version of another earlier radiated magnetic emission model [3]. A few model parameters must be, nevertheless, provided for any model extraction. In this model, the length and position of every dipole are pre-fixed, and the orientation of each dipole, and their currents are extracted. The model implements a state-of-the-art extraction technique to determine the three unknown model parameters: real, imaginary part of the dipole currents, and the dipole orientations. It takes into account the importance of ϵ_{reff} during extraction; it has to be provided as an input parameter before model extraction. The parameters are extracted with the use of an iterative optimization algorithm based on the Levenberg-Marquardt technique. The model calculates the radiated electromagnetic fields of any device under test at any height above it. The complete details of the model, along with its extraction procedure are detailed in [4].
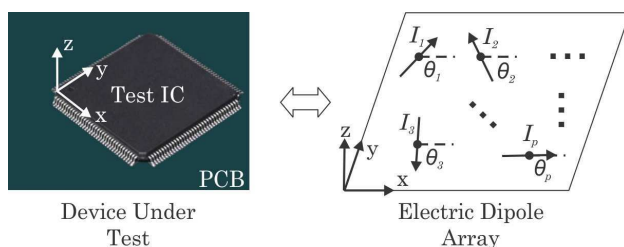

Figure 1. Electric dipole array representing the model.

2.2. Mathematical Improvements

Though the model is way more versatile and stable than the earlier models, it suffers from a few disadvantages:

- As the device under test becomes large and complex, thereby requiring a large number of dipoles to accurately predict the radiated electromagnetic fields, model extraction requires large computational resources and is time consuming.
- The knowledge of the substrate details (ϵ_{reff}) is needed prior to extraction.
- If the device under test has multiple substrates (which is the case with most practical devices), ϵ_{reff} is not a constant at all points in space above the device.
- The number of dipoles used for modeling is not optimized.

A number of mathematical improvements have been made to the existing extraction procedure in order to overcome these disadvantages. They are individually explained below:

(i) Several model applications on a variety of microwave devices like a microstrip line, miniature and on-chip devices in [4, 5] show us that the modeling time is relatively larger as opposed to the model in [3]. As a typical example, the time to extract the model parameters for an "on-chip" patch antenna with 240 dipoles was around 17 minutes, though the model in [3] extracts the parameters in 2.5 minutes. Though the loss of speed is more than made up with the gain in model versatility and robustness, we feel that it could become computationally very intensive if the device-to-be modeled becomes complex and the number of dipoles go above 600–700. The mathematics behind model extraction has thus been tweaked and improved to overcome probable computational failures by the inclusion of the "System Jacobian Matrix" within the optimization procedure.

(ii) The next important aspect is the determination of ϵ_{reff} of the device under test. It is not always possible to know its value beforehand. Moreover, if there are multiple substrates in a single device, it becomes impossible to determine the effective value. It is thus proposed to extract its value at all measurement points so that its knowledge prior to extraction is no more mandatory. An optimization procedure based on the Levenberg-Marquardt technique is used for this purpose.

(iii) Another significant advancement has been made to optimize the number of dipoles needed to build an accurate model. Keeping the core system intact, the dipole positions are directly determined

from the radiated near-magnetic field measurements, based on the use of thresholding and windowing technique. The former is used to locate the dipoles and the latter to optimize the number of dipoles in a particular window of the measured field. With this addition, the modeling pre-requisite is the dipole length alone.

3. MODEL EXTRACTION

A cutting-edge extraction procedure, inspired from the modeling procedure in [4], has been developed so as to extract the model. The following parameters of the model need to be determined: dipole positions, their orientations ($\theta \in \mathbb{R}$), currents ($I \in \mathbb{C}$) and the effective relative permittivity ($\epsilon_{reff} \in \mathbb{R}$) of the device under test. The heuristic methodology is implemented in MATLAB and is explained in this section.

3.1. Determining Dipole Positions

The first step of model construction is determining the positions where the dipoles constituting the model are to be placed. The intensity thresholding technique is used to locate the points where the field is significant [10]. The tangential components of the measured near-magnetic field are used for this purpose. An intensity value is used to differentiate the low and high field points. The objective behind the thresholding procedure is to "binarize" the field data and separate them into two basic clusters: one containing the significant field points (represented as 1), other representing the noise and low field points (represented as 0). The user is allowed to choose the intensity values for the field components independently. The default intensity value is calculated using the Otsu's method, pre-coded in MATLAB. It is found from many of our trials that the Otsu's method, though one of the most commonly used thresholding method in the Image processing industry, does not always give sufficient details for model construction. To further optimize the number of dipoles, the windowing technique can be optionally used to split the field into n parts. Again, the user can select n depending on the field distribution. This would facilitate to control the intensity level and thereby detect the dipole position in each selected window.

3.2. System Formulation

The core of non-linear system in [4] is slightly modified to extract the all the model parameters. Based on a detailed study on the role of ϵ_{reff}

on the radiated electromagnetic fields, it is inferred that its effect is negligible on the magnetic field very close to the device under test and mostly felt on the electric field at any point in space [4]. The normal component of the electric field is thus used in addition to the tangential magnetic field components to aid the extraction process. The system is represented in a matrix form denoting the radiations of every dipole in the model at a particular point of interest as shown below:

$$
\begin{aligned}
[H_x] &= f_{Hx}\left([\alpha_x], [I_r], [I_i], [\theta], [k], fr\right) \\
[H_y] &= f_{Hy}\left([\alpha_y], [I_r], [I_i], [\theta], [k], fr\right) \\
[E_z] &= f_{Ez}\left([P_0], [P_d], [I_r], [I_i], [\theta], [k], [\epsilon], fr\right)
\end{aligned}
\tag{1}
$$

where, $[\theta] \in \mathbb{R}$ represents the orientations of the dipoles, $[I_r] \in \mathbb{R}$ is the real part of the dipole currents, $[I_i] \in \mathbb{R}$ corresponds to the imaginary part of the dipole currents, fr is the modeling frequency, $[\alpha_x]$ and $[\alpha_y]$ are calculated based on the dipole positions, their lengths and the observation point, $[\epsilon]$ is the medium's permittivity given by $[\epsilon_0 \epsilon_{reff}]$, ϵ_0 is the permittivity of free space ($8.85418 \times 10^{-12}\,\mathrm{F/m}$), $[\epsilon_{reff}]$ is the effective relative dielectric constant of the DUT, $[k]$ is the wave number given by $[k] = (2\pi/\lambda) \times [\epsilon_{reff}]^{0.5}$, with λ (wavelength) $= c/fr$ where c is the velocity of light in air, $[P_d]$ is the dipole position vector, $[P_0]$ is the position vector of the observation point, and f_{Hx}, f_{Hy}, and f_{Ez} are non-linear mathematical functions associating all the other parameters and variables. $[\theta]$, $[I_r]$, $[I_i]$ of the dipoles and $[\epsilon_{reff}]$ at each observation point are the parameters to be extracted.

3.3. Initial Parameter Vector

In any iterative model, the initial parameter estimate is a very important step in determining the range and validity of the model parameters. They can either be calculated mathematically or determined analytically. The initial values of the dipole parameters ($[I_r^{init}]$, $[I_i^{init}]$, $[\theta^{init}]$) are calculated with the use of "matrix inverse method" as shown by the following equations [4]:

$$
\begin{aligned}
[\theta^{init}]_{p \times 1} &= f_\theta \left([\alpha_x]^{-1}_{m \times p}, [H_x]_{m \times p}, [\alpha_y]^{-1}_{m \times p}, [H_y]_{m \times p}\right) \\
[I_r^{init}]_{p \times 1} &= g_a \left([\theta^{init}]_{p \times 1}, real\left\{[H_x]_{m \times p}\ or\ [H_y]_{m \times p}\right\}\right) \\
[I_i^{init}]_{p \times 1} &= g_b \left([\theta^{init}]_{p \times 1}, imag\left\{[H_x]_{m \times p}\ or\ [H_y]_{m \times p}\right\}\right)
\end{aligned}
\tag{2}
$$

where, m is the number of measurement points, p is the number of dipoles used for modeling, and f_θ, g_a, and g_b are mathematical functions. Mathematically, the inversion can be performed for square matrices. If $m \neq p$, the pseudo-inverse technique based on the orthogonal transformation method is used for calculation. It is

important to note that $[\theta^{init}]$ is determined irrespective of the dipole currents and moreover, the tangential magnetic field components of the near-magnetic field alone are sufficient for its estimation. The real and imaginary parts of the dipole currents are then extracted from $[\theta^{init}]$. The choice of the field component for its extraction (H_x or H_y) depends on which ever between them is significant. Nevertheless, a good estimate is obtained on choosing H_x or H_y, but their choice must be consistent in determining both $[I_r^{init}]$ and $[I_i^{init}]$. The initial estimate for the last parameter $[\epsilon_{reff}^{init}]$ is a unity vector ($= 1$) considering the physical fact that the relative permittivity of vacuum is 1. It is also equally essential to mention that the minimum value of ϵ_{reff} is also 1.

3.4. The Optimization Algorithm

The initial parameters are passed through a two-level Levenberg-Marquardt optimization algorithm, which is the most widely used iterative procedure for non-linear optimization. It simply outperforms the gradient descent algorithm or other conjugate gradient methods [11, 12]. The algorithm uses a damping factor (μ) which influences both the direction and the parameter step size (h_{lm}). For non-linear systems, the Jacobian matrix is indispensable for determining the best-available roots. It can be either be predetermined or dynamically calculated. The damping parameter and the step size can be calculated directly from the Jacobian matrix (J), using the following equation:

$$\left(J^T J + \mu I\right) h_{lm} = -J^T f, \quad \mu \geq 0. \tag{3}$$

Here $f = f(x)$ defines the non-linear system. In the previous model, the Jacobian matrix was calculated using the finite difference method. It is important to mention that the calculation of this matrix is computationally intensive, due to its mere size. The procedure becomes vulnerable to errors when the system becomes large and complex. To speed up the modeling time, and avoid any possible error, we propose to predetermine the Jacobian. The Jacobian matrix, as we all know, is defined as the matrix of all first-order derivatives of a vector or scalar valued function with respect to another vector. For m real-valued functions such as $y_1(x_1, x_2, \ldots, x_n)$, $y_2(x_1, x_2, \ldots, x_n)$, $\ldots$,

$y_m(x_1, x_2, \ldots, x_n)$, the Jacobian is defined by:

$$J_F = \begin{bmatrix} \dfrac{\partial y_1}{\partial x_1} & \dfrac{\partial y_1}{\partial x_2} & \cdots & \dfrac{\partial y_1}{\partial x_n} \\ \dfrac{\partial y_2}{\partial x_1} & \dfrac{\partial y_2}{\partial x_2} & \cdots & \dfrac{\partial y_2}{\partial x_n} \\ \vdots & \vdots & \ddots & \vdots \\ \dfrac{\partial y_m}{\partial x_1} & \dfrac{\partial y_m}{\partial x_2} & \cdots & \dfrac{\partial y_m}{\partial x_n} \end{bmatrix} \tag{4}$$

It is computationally very intensive to calculate all the model parameters simultaneously because of the dimensions of the Jacobian involved. So, we propose to break up the optimization into two-levels: the first-level to optimize the dipole parameters and the second-level optimization to extract ϵ_{reff} at all measurement points.

3.4.1. Level 1: Optimizing Dipole Parameters

As stated earlier, the role of the effective relative permittivity is negligible on the magnetic field very close to the device under test and mostly felt on the electric field at any point in space. Considering this, the dipole parameters can first be extracted by neglecting ϵ_{reff} in their calculations, since they can be directly extracted from the near-magnetic field measurements. By the term "neglecting," we mean that $\epsilon_{reff} = 1$ at all points in space. The optimization function for this level is given by:

$$f_1 = \begin{cases} real(H_x^{model}) - real(H_x^{meas.}) \\ imag(H_x^{model}) - imag(H_x^{meas.}) \\ real(H_y^{model}) - real(H_y^{meas.}) \\ imag(H_y^{model}) - imag(H_y^{meas.}) \end{cases} \tag{5}$$

where,

$$\begin{aligned} \left[H_x^{model}\right] &= f_{Hx}\left([\alpha_x], [I_r^{iter}], [I_i^{iter}], [\theta^{iter}], [k], fr\right) \\ \left[H_y^{model}\right] &= f_{Hy}\left([\alpha_y], [I_r^{iter}], [I_i^{iter}], [\theta^{iter}], [k], fr\right) \end{aligned}$$

with $[k] = (2\pi/\lambda)$ at all measurement points, and $[\theta^{iter}], [I_r^{iter}], [I_i^{iter}]$ are updated parameter values on each iteration ($= [\theta^{init}], [I_r^{init}], [I_i^{init}]$ respectively for the first iteration). Every equation in the optimization function is a real-valued function of the dipole orientations and the

currents, it is possible to define the Jacobian as:

$$J_{F1} = \begin{bmatrix} \frac{\partial(t_1,t_2,\cdots,t_m)}{\partial(I_{r1},I_{r2},\cdots,I_{rp})} & \frac{\partial(t_1,t_2,\cdots,t_m)}{\partial(I_{i1},I_{i2},\cdots,I_{ip})} & \frac{\partial(t_1,t_2,\cdots,t_m)}{\partial(\theta_1,\theta_2,\cdots,\theta_p)} \\ \frac{\partial(u_1,u_2,\cdots,u_m)}{\partial(I_{r1},I_{r2},\cdots,I_{rp})} & \frac{\partial(u_1,u_2,\cdots,u_m)}{\partial(I_{i1},I_{i2},\cdots,I_{ip})} & \frac{\partial(u_1,u_2,\cdots,u_m)}{\partial(\theta_1,\theta_2,\cdots,\theta_p)} \\ \frac{\partial(v_1,v_2,\cdots,v_m)}{\partial(I_{r1},I_{r2},\cdots,I_{rp})} & \frac{\partial(v_1,v_2,\cdots,v_m)}{\partial(I_{i1},I_{i2},\cdots,I_{ip})} & \frac{\partial(v_1,v_2,\cdots,v_m)}{\partial(\theta_1,\theta_2,\cdots,\theta_p)} \\ \frac{\partial(w_1,w_2,\cdots,w_m)}{\partial(I_{r1},I_{r2},\cdots,I_{rp})} & \frac{\partial(w_1,w_2,\cdots,w_m)}{\partial(I_{i1},I_{i2},\cdots,I_{ip})} & \frac{\partial(w_1,w_2,\cdots,w_m)}{\partial(\theta_1,\theta_2,\cdots,\theta_p)} \end{bmatrix} \quad (6)$$

where, $(t_1, t_2, \cdots, t_m)$, and $(u_1, u_2, \cdots, u_m)$, corresponds to the real and imaginary parts of H_x field, and $(v_1, v_2, \cdots, v_m)$, and $(w_1, w_2, \cdots, w_m)$, corresponds to the real and imaginary part of the H_y field respectively. This matrix gives us the best non-linear approximation of the model, for the given initial parameters. The Jacobian is so carefully coded such that its evaluation is quick and memory efficient. For every step in the iterative process, the Jacobian is determined to evaluate the step size (h_{lm}) in (3).

As reported by Moré [13], the simplest way to obtain h_{lm} is to use the Cholesky decomposition. But it is highly unreliable when $\mu = 0$ and the rank of the Jacobian is deficient. Alternate techniques are to use the QR decomposition method, and the orthogonal transformation method. Though the former provides the most accurate solution, we prefer to use the orthogonal transformation method for one main reason: it is computationally cheaper than the QR method since the determination of h_{lm} is just a step in the algorithm and need not be calculated with very high accuracy. When the system becomes too large, the loss in speed with the QR method is very significant and requires large computational resources. The orthogonal transformation is an excellent, reliable and robust alternative. Given in an iteration, if the orthogonal transformation method is not applicable (if the matrix is singular or rank deficient), the code automatically computes the step size using the QR decomposition method, for that iteration alone.

3.4.2. Level 2: Optimizing ϵ_{reff}

With the optimized dipole parameters, the next step is to determine the last unknown parameter, ϵ_{reff} at all measurement points. The optimization function for this level, similar to that of level 1, is separated into real and imaginary parts as:

$$f_1 = \begin{cases} real\left(E_z^{model}\right) - real\left(E_z^{meas.}\right) \\ imag\left(E_z^{model}\right) - imag\left(E_z^{meas.}\right) \end{cases} \quad (7)$$

where,

$$\left[E_z^{model}\right] = f_{Ez}\left([P_0], [P_d], \left[I_r^{optim}\right], \left[I_i^{optim}\right], [\theta^{optim}], [k^{iter}], [\epsilon^{iter}], fr\right),$$

with $[\theta^{optim}]$, $[I_r^{optim}]$, $[I_i^{optim}]$ being the optimized parameters from level 1, $[k^{iter}] = (2\pi/\lambda) \times [\epsilon_{reff}^{iter}]^{0.5}$ and $[\epsilon^{iter}] = [\epsilon_0 \epsilon_{reff}^{iter}]$, $[\epsilon_{reff}^{iter}]$ is updated on every iteration $(= [\epsilon_{reff}^{init}]$ for the first iteration). The Jacobian for this system is determined to be:

$$J_{F2} = \left[\begin{array}{c} \frac{\partial(t_1, t_2, \cdots, t_m)}{\partial(\epsilon_{r1}, \epsilon_{r2}, \cdots, \epsilon_{rp})} \\ \frac{\partial(u_1, u_2, \cdots, u_m)}{\partial(\epsilon_{r1}, \epsilon_{r2}, \cdots, \epsilon_{rp})} \end{array} \right] \tag{8}$$

where, $(t_1, t_2, \cdots, t_m)$, and $(u_1, u_2, \cdots, u_m)$, corresponds to the real and imaginary parts of E_z field. As discussed with the level 1 optimization, the step size of each iteration is calculated using the orthogonal transformation method. The QR decomposition technique is optionally used in case the orthogonal transformation method does not solve for the step size. One important feature is that this level is "height" independent, i.e., E_z need not be measured at the same height as that of H_x and H_y. The model extraction algorithm is explained in a simplified manner in the flowchart in Figure 2.
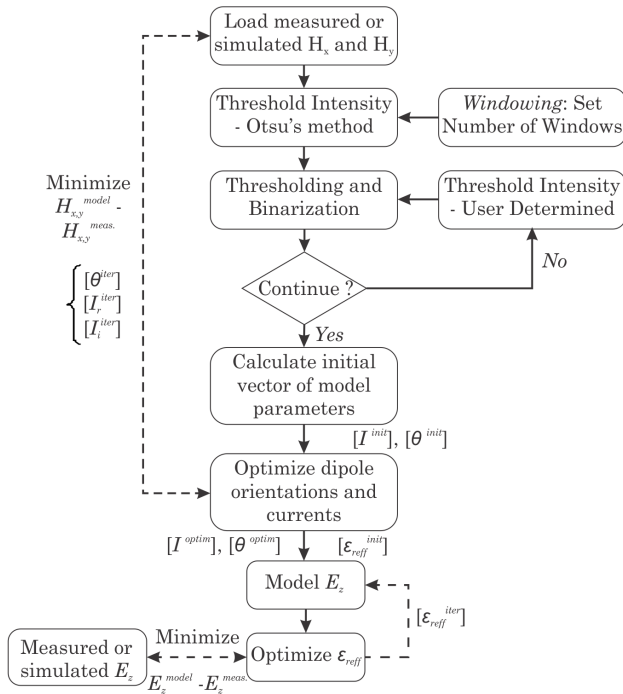

**Figure 2.** The modeling algorithm.

4. MODEL APPLICATION AND VALIDATION

The new modeling technique is applied and validated on a few commonly used microwave devices, simple and complex. Simple devices are those that contain a single uniform substrate and complex devices contain multiple substrates. The advantage of the automatic dipole detection technique, with and without the use of the windowing technique is discussed. For complex devices, the windowing technique is used for optimizing the number of dipoles in the model so that the computation is memory efficient. All the models are built on a PC, with 3.2 GHz Dual Core Processor and 3.2 GB physical RAM.

4.1. Simple Test Cases

First, the model is applied on a 90° hybrid coupler, operating at 1 GHz. The near-tangential magnetic fields are measured using the test bench in IRSEEM, similar to those made in [4, 14], at a height of 1.5 mm above the coupler. A differential loop probe of 3.14 mm^2 is used for this purpose [4]. The near-normal electric field is measured using a monopole probe at 2.5 mm above the coupler (coupling between the probe and the DUT is significant at distances lesser than 2.5 mm). Using the automatic dipole detection technique, with dipole length set to 1 mm, without the windowing technique, a set of 384 dipoles is detected with the intensity level set to 6% for H_x and H_y. This is about 30% less than the number of dipoles used with the previous method [4]. The intensity level was decided on various trial and error methods and it was found that an intensity level in the range [4–10%] provides sufficient number of dipoles for accurate modeling. On applying the windowing technique, with six windows selected by judging the near-magnetic field cartographies, 330 dipoles (each of length 1 mm) are detected with [70%, 70%, 8%, 9%, 80%, 80%] intensity values on each window for H_x and [8%, 9%, 70%, 70%, 7%, 7%] for H_y. Locations in which the fields are in-significant (in H_x and H_y) are set to high intensity levels. The detected dipoles are shown along with the detected $|H_{xy}|$ field ($H_{xy} = \sqrt{H_x^2 + H_y^2}$) in Figure 3. The window borders are shown as a dotted rectangle. The advantage of the automatic dipole detection technique can be easily understood with the help of the above example.

The dipole parameters (level 1) are extracted in span of 68 seconds as opposed to 14.5 minutes taken by the previous extraction procedure; the second level optimization converges in 178.2 seconds. The speed up is fundamentally due to the efficient Jacobian calculation as against to the finite difference method. Thus the total modeling time is about
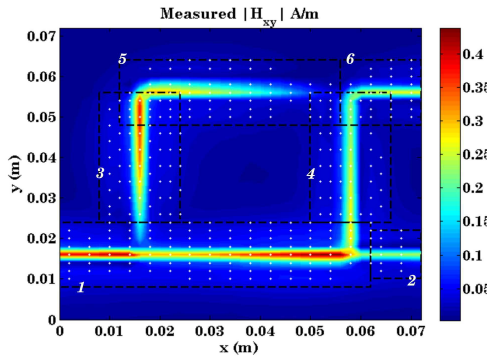
Figure 3. Automatically detected dipoles in each window for a hybrid coupler.
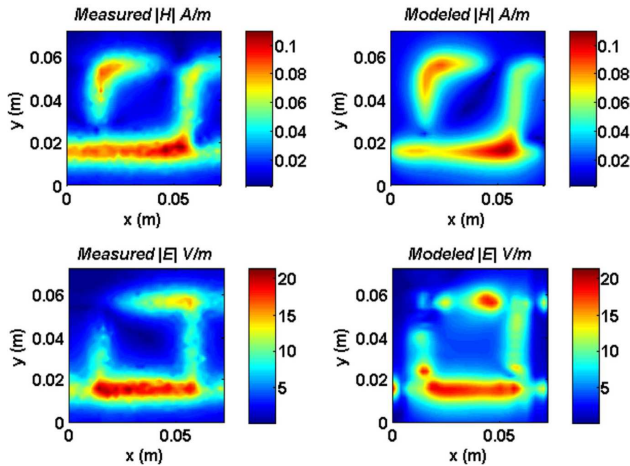
Figure 4. Modeled electromagnetic fields in comparison with those of measurements (and simulations) at 5 mm above the coupler. The H_x, H_y, H_z and E_z fields are measured using the test-bench and E_x and E_y quantities are obtained from HFSS simulations.

4.5 minute with a set of 330 dipoles. The mean value of ϵ_{reff} in all the windows, where the fields are significant is about 3.58 as against the empirical value 3.4, with a tolerable relative error of 5.3%. The model is simulated at 5 mm above the coupler and the modeled fields are compared with those of measurements (and simulations) in Figure 4. In fact, the measurement of the tangential electric field components (E_x and E_y) is still under study in IRSEEM [15], and thus Ansoft HFSS
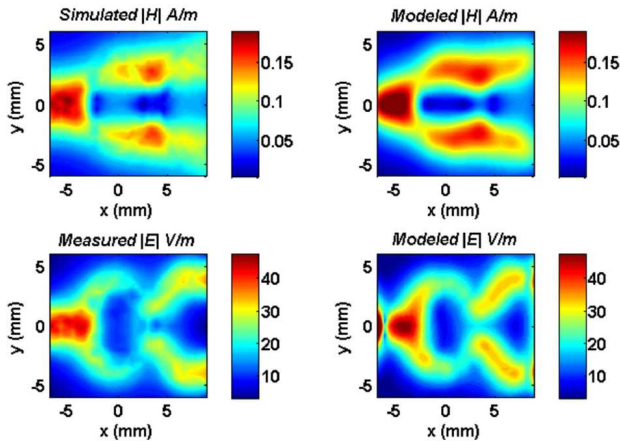
Figure 5. Validation of the modeled electromagnetic fields with those of HFSS simulations on the Wilkinson power divider at 1.5 mm above the device.

simulations of the coupler are used in tandem for validation purpose alone. Therefore, the term "Measured" in Figure 4 is a misnomer; the field quantities contain both the measured (H_x, H_y, H_z and E_z) and HFSS simulated fields (E_x and E_y). The model is then applied to a balanced Wilkinson power divider operating at 5.6 GHz, predominantly used for feeding a Wi-Fi antenna array structure. Due to the non availability of near-field probes capable of functioning at 5.6 GHz, the device is designed and simulated in Ansoft HFSS and the radiated fields at 500 μm above the device is used for constructing the model. 478 dipoles are automatically detected in a single window, covering the entire device, length of each dipole = 250 μm. The extraction of all the parameters takes 7.3 minutes and the extracted ϵ_{reff} (2.75) is in close agreement with the empirical values (2.81). The radiated electromagnetic fields are simulated at 1.5 mm above the divider and the results are compared with those of HFSS simulations in Figure 5.

4.2. Complex Test Case

To validate the proof of concept, a test device built on multiple substrates is designed. The above validated Wilkinson power divider is intended to feed two other high frequency transmission lines as shown in Figure 6; both the transmission lines are excited with the same power. The power divider is built on a Roger RO4003 substrate of height 400 μm and $\epsilon_r = 3.55$, the microstrip line 1 is
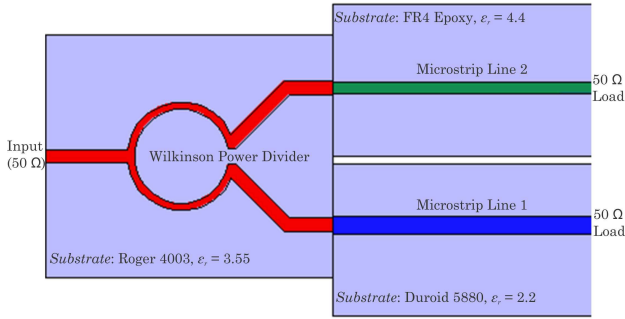
**Figure 6.** The designed complex device operating at 5.6 GHz. The design is intended as a proof of concept.
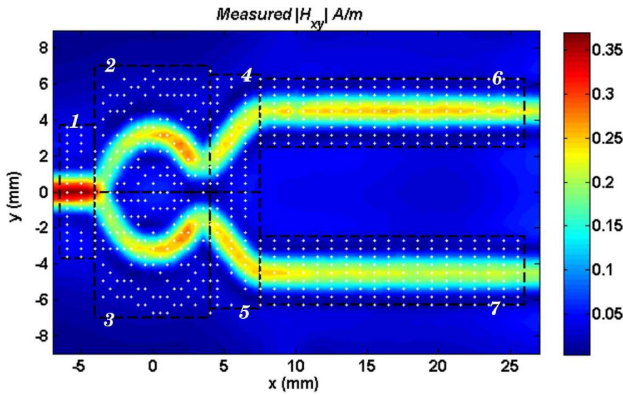
Figure 7. The detected dipoles and the windows used for modeling the complex device.

built on a Duroid 5880 substrate of height $400 \, \mu m$ and $\epsilon_r = 2.2$ and microstrip line 2 is built on a FR4 epoxy substrate of height $400 \, \mu m$ and $\epsilon_r = 4.4$. The system operates at $5.6 \, GHz$ and possesses a characteristic impedance of $50 \, \Omega$, the power divider is fed with a power of $0 \, dBm$ ($1 \, mW$) and the transmission lines are terminated with $50 \, \Omega$ load impedances. The device is simulated in Ansoft HFSS and the radiated fields at $1 \, mm$ above the device is used to build the model. Deciding "by sight," the fields are split into seven unique windows; the intensity levels of $[90\%, 8\%, 8\%, 7\%, 7\%, 80\%, 80\%]$ is set for H_x field and $[11\%, 8\%, 8\%, 11\%, 11\%, 6\%, 7\%]$ for H_y field respectively. The total tangential magnetic field (H_{xy}) is shown along with the detected dipoles in Figure 7. It is important to state that the number of dipoles

representing the power divider (Windows 1–5) is 338, as opposed to 478 dipoles when validated singleton. This difference (29.3%) is in-fact very significant in such devices with "non-collinear" field distribution when compared to that found in devices like the above validated coupler. This is the major advantage using the automatic detection process, with windowing enabled. The system is modeled with a set of 680 dipoles, each of length 250 μm. The level 1 optimization takes 7 minutes and 40 seconds to converge and level 2 takes 278 seconds, and thus all the model parameters are extracted in a span of 12 minutes and 20 seconds. The extracted ϵ_{reff} in each window is tabulated in Table 1. The dipole network representing the model is shown in Figure 8.
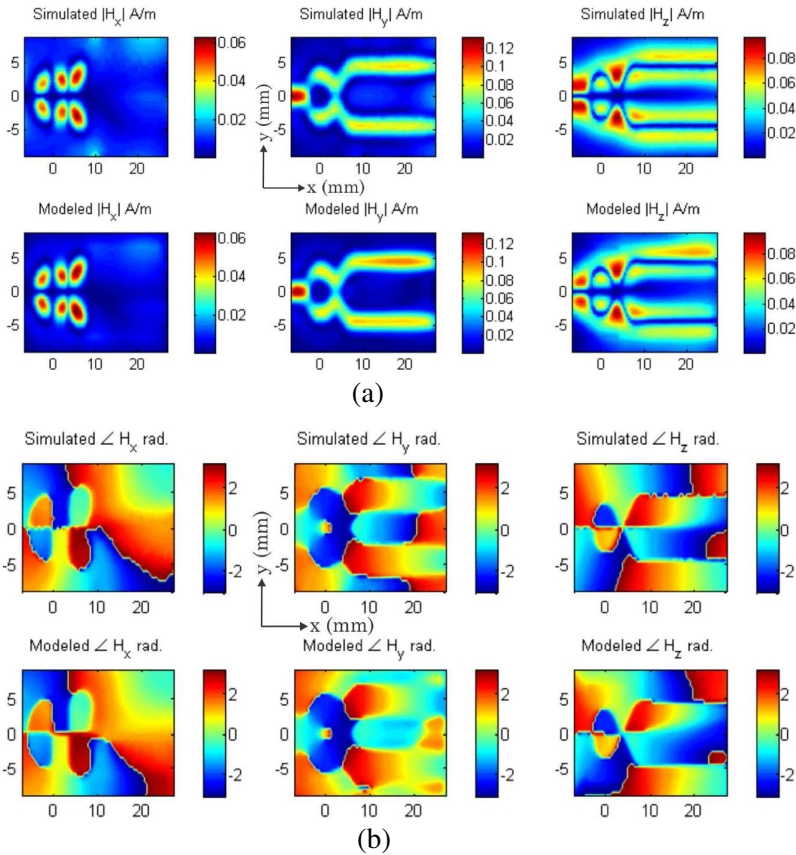
The electromagnetic fields at 2 mm above the device is then simulated and compared with those of HFSS results in Figure 9 and
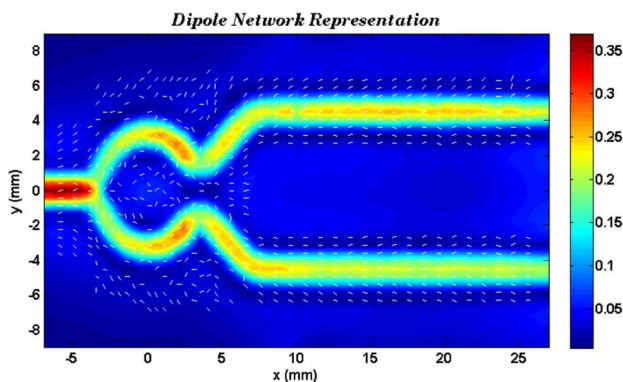
Figure 8. The extracted dipoles are plotted coherently with the measured total tangential field at 5.6 GHz. The white marks represent the dipoles, each of length 250 μm.

Table 1. The extracted ϵ_{reff} values for the complex device.

| Window No.	Extracted ϵ_{reff} (empirical)	Relative error (%)
1	2.62 (2.75)	4.7%
2	2.77 (2.75)	0.73%
3	2.80 (2.75)	1.82%
4	2.92 (2.75)	6.1%
5	2.88 (2.75)	4.7%
6	3.32 (3.27)	1.5%
7	1.91 (1.84)	3.8%

Figure 9. Comparison between the modeled magnetic fields with those of HFSS simulations at 2 mm above the device (a) magnitude comparison, (b) phase comparison.

Figure 10. Excellent correlation is found for the magnitude and phase of the electric and magnetic fields between the modeled and simulated results. There are certain errors in optimizing the model parameters in the regions where the fields are insignificant; nevertheless, these components do not affect the total radiated fields.

4.3. Summary

Table 2 summarizes the validation of the model on all the test devices. It is interesting to note that the modeling technique is rapid and robust. It is important to mention that the coupler, with optimized number of dipoles takes a longer time to converge than that without the using the
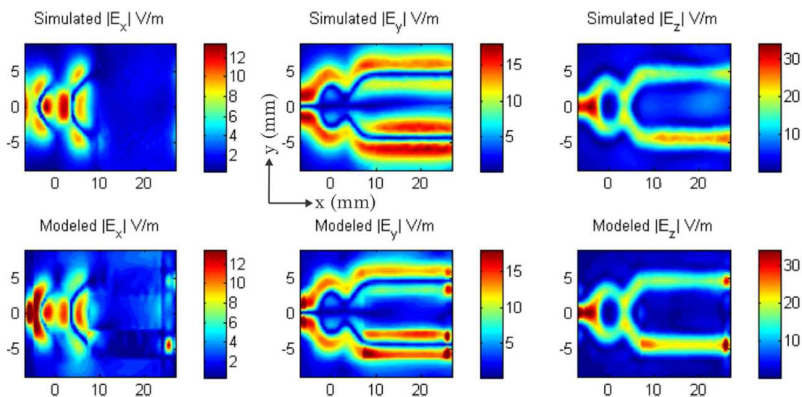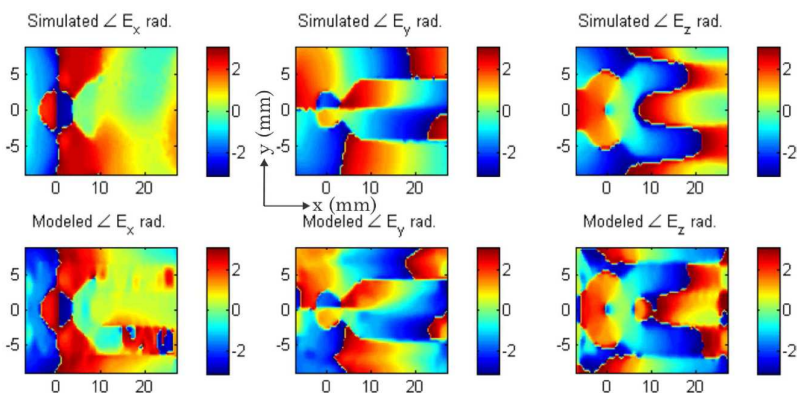
Figure 10. Comparison between the modeled electric fields with those of HFSS simulations at 2 mm above the device (a) magnitude comparison, (b) phase comparison.

windowing technique; this is primarily due to rank deficiency problems faced by the solver during certain iterations. Under those conditions, as previously stated, the solver uses the QR technique to solve the system and thus takes a much longer time. Nevertheless, lesser the dipoles used to build the model, easier and faster it is to integrate it into commercial tools at a later time as reported in [8, 9].

The greatest advantage of the new solver is its capability to solve large and complex systems rapidly and efficiently. In the case of the complex text case, with a set of 680 dipoles, the solver is tremendously fast than the one previously developed [4]. As stated in [5], the extraction takes about 45 minutes in cases of using 700 dipoles. In

Table 2. Model validation summary on all the test devices.

Device Under Test	Window-ing	No. of Dipoles	Dipole Opt-imization %	Computational Time[a]
Hybrid Coupler	off	384	NA	3'12"
	on	330	14%	4'30"
Wilkinson Power Divider	off	478	NA	3'31"
	on	338[b]	29.3%	NA
Complex Device	off	NA	NA	NA
	on	680	NA	12'20"

[a] All tests were performed on a PC, with 3.2 GHz Dual Core Processor and 3.2 GB physical RAM.
[b] Number of dipoles representing the power divider in the complex circuit (window 1–window 5).

fact, we could not solve the complex device with the previous method due to memory allocation problems encountered, caused merely due to the size of the model (measurement points and number of dipoles) involved with the finite difference Jacobian.

5. CONCLUSION

A fast and robust electromagnetic radiated emission model, represented with a set of elementary electric dipoles has been developed in this paper. With such an implementation, all the constraints of the erstwhile model have been overcome and a breakthrough has been achieved with respect to model performance. The model, deploying a cutting-edge extraction procedure, predicts the radiated electromagnetic emissions at any height above the device under test in quick time. The prerequisites for modeling are the measured or simulated tangential near-magnetic field and the normal near-electric field. An additional module implementing the thresholding and windowing techniques optimizes the number of dipoles needed for accurate modeling.

The two-level, fine-tuned optimization procedure extracts the dipole parameters and the effective relative permittivity at all points in space, preserving their physical sense. For each level, the system is separated into real and imaginary parts and optimized simultaneously, with their corresponding Jacobians predefined. The smart procedure chooses between the orthogonal transformation technique and the QR decomposition technique to determine the step size in each iteration. This offers significant improvement in modeling speed and reliability. The model is validated on a couple of simple devices

built on a single substrate and a complex device consisting multiple substrates. Excellent results have been obtained for the modeled fields in comparison with measurements and/or simulations for all the test devices. The extracted effective relative permittivity correlates well with those for empirical calculations in all the cases. The model speed and performance have also been discussed. The varied dimensions of the validated devices and their wide frequency range gives us an idea of the model's capability, scalability and versatility. The model is simple in its implementations and offers easy availability to electronic designers. Being a generic model, it can be applied to any component, active and passive. The optimized number of dipoles facilitates better integration into commercial 3D simulation tools such as Ansoft HFSS as reported in [8, 9].

ACKNOWLEDGMENT

REFERENCES

1. Labussière-Dorgan, C., S. Bendhia, E. Sicard, J. Tao, H. J. Quaresma, C. Lochot, and B. Virgnon, "Modeling the electromagnetic emission of a microcontroller using a single model," *IEEE Trans. Electromagn. Compat.*, Vol. 50, 22–34, Feb. 2008.

2. Sicard, E., A. Boyer, and A. Tankielun, "On the prediction of near-field microcontroller emissions," *IEEE Int. Symp. Electromagn. Compat.*, Chicago, USA, Aug. 2005.

3. Vives, Y. G., C. Arcambal, A. Louis, F. de Daran, P. Eudeline, and B. Mazari, "Modeling magnetic radiations of electronic circuits using near-field scanning method," *IEEE Trans. Electromagn. Compat.*, Vol. 49, 391–400, May 2007.

4. Ramanujan, A., Z. Riah, A. Louis, and B. Mazari, "Modeling the electromagnetic radiations of passive microwave components using a near-field scanning method," *IEEE Trans. Electromagn. Compat.*, Vol. 52, No. 4, 1056–1059, Nov. 2010.

5. Ramanujan, A., Z. Riah, A. Louis, and B. Mazari, "On the radiated emission modeling of on-chip microwave components," *IEEE Int. Sym. Electromagn. Compat.*, Florida, USA, Jul. 2010.

6. Fernández, P. L., C. Arcambal, S. Verdeyme, D. Baudry, and B. Mazari, "Near-field measurements to create a model suitable for a commercial simulation tool," *4th Inter. Conf. Electromagn. NF Charac. Imaging (ICONIC)*, 208–213, Taipei, Jun. 2009.

7. Fernández, P. L., C. Arcambal, S. Verdeyme, D. Baudry, and B. Mazari, "Radiation modeling and electromagnetic simulation of an active circuit," *7th Int. Work. EMC IC (EMC Compo 09)*, No. 58, Toulouse, France, Nov. 2009.

8. Fernández, P. L., A. Ramanujan, Y. Vives-Gilabert, C. Arcambal, A. Louis, and B. Mazari, "A radiated emission model compatible to a commercial electromagnetic simulation tool," *20th Int. Sym. Electromagn. Compat.*, Zurich, Jan. 2009.

9. Fernández, P. L., C. Arcambal, Y. Vives-Gilabert, A. Ramanujan, D. Baudry, A. Louis, and B. Mazari, "Development of a magnetic field model and insertion into a commercial electromagnetic simulator," *Turk. J. of Elec. Eng. Comp. Sci.*, Vol. 17, No. 3, 289–300, 2009.

10. Sezgin, M. and B. Sankur, "Survey over image thresholding techniques and quantitative performance evalua-tion," *Journal Electronic Imaging*, Vol. 13, No. 1, 146–165, Jan. 2004.

11. Levenberg, K., "A method for the solution of certain problems in least squares," *Quart. Appl. Math.*, Vol. 2, 164–168, 1944.

12. Marquardt, D., "An algorithm for least-squares estimation of nonlinear parameters," *SIAM J. Appl. Math.*, Vol. 11, 431–441, 1963.

13. Moré, J. J., "The Levenberg-Marquardt algorithm: Implementation and theory," *Lecture Notes in Mathematics*, Vol. 630, 105–116, Springer, 1978.

14. Baudry, D., C. Arcambal, A. Louis, B. Mazari, and P. Eudeline, "Applications of the near-field techniques in EMC investigations," *IEEE Trans. Electromagn. Compat.*, Vol. 49, No. 3, Aug. 2007.

15. Bouchelouk, L., Z. Riah, D. Baudry, M. Kadi, A. Louis, and B. Mazari, "Characterization of electromagnetic fields close to microwave devices using electric dipole probes," *Inter. J. RF Micro. Comp. Aid. Eng.*, Vol. 18, 146–156, Mar. 2008.